Phased Array With Pattern Shaping and Scan Loss Reduction for Millimeter Waves

van Schelven, Ralph; Syed, Waqas; Carluccio, Giorgio ; Doris, Kostas ; de Graauw, Anton; Neto, Andrea ; Cavallo, Daniele

DOI
10.1109/TAP.2022.3217340

Publication date
2023

Document Version
Final published version

Published in
IEEE Transactions on Antennas and Propagation

Phased Array With Pattern Shaping and Scan Loss Reduction for Millimeter Waves

Ralph M. van Schelven, Waqas H. Syed, Giorgio Carluccio, *Member, IEEE*, Kostas Doris, *Member, IEEE*, Anton de Graauw, Andrea Neto, *Fellow, IEEE*, and Daniele Cavallo, *Senior Member, IEEE*

***Abstract*— In this work, we investigate antenna architectures to implement dual-mode operation in phased array designs. Planar slot antenna elements are used in array configuration, in combination with artificial dielectrics layers (ADLs) located in the close proximity of the array, to achieve pattern shaping. The artificial dielectric superstrate supports the propagation of leaky waves that can be optimized to enhance the gain in a specific angular region or to enlarge the array field of view. By controlling the amplitude and phase of the antenna elements, the radiation patterns can be combined to realize either wide or narrow beams. This concept present advantages for both millimeter-wave (mm-wave) communication and radar applications. A design of a four-element array fabricated in standard printed circuit board (PCB) technology validates the feasibility of the dual-mode operation. The measured results also show good agreement with simulations.**

***Index Terms*— Artificial dielectric layers (ADLs), leaky waves, millimeter-waves (mm-waves), pattern diversity, pattern shaping, phased array.**

I. Introduction

IN MILLIMETER-WAVE (mm-wave) communication and radar applications, radiation pattern diversity has become an attractive property for the antenna systems. For example, base stations in wireless cellular networks will comprise antenna arrays that can switch between narrow or wide beams to achieve optimal capacity for different user distributions [1]. Multimode operation of antennas that can dynamically change the radiation beamwidth allow to reuse for multiple purposes the limited number of output channels available from mm-wave integrated circuits (ICs). Another advantage of implementing a single antenna system with a variable beamwidth is the smaller area usage compared with two separate antennas. The multimode operation can be simply achieved with digital excitation of antennas operating in free space. However, for well-defined scenarios where the beam efficiency is important (the radiated power needs to be within $\pm\theta_{\text{design}}$), the use of wide angle impedance matching (WAIM) that support leaky waves can be beneficial. The leaky waves that propagate along the structure can focus the radiation in some desired directions [2]. Specifically here, we target a double-operation mode scenario. For one mode of operation side, we aim at a phased array capable of maintaining high gain over a wider scan range, up to $\pm 45°$. The same array should also be able to generate a single beam with a beamwidth up to $\pm 45°$.

The two modes of operation would not be simply realized with an array in free space, while a superstrate supporting a leaky wave aiming at roughly $\theta_{\text{design}} = \pm 45°$ can facilitate them both. In fact, phased arrays in free space are characterized by scan loss, i.e., a reduction of gain as a function of scan angle. It is known that a WAIM layer such as the one originally proposed in [3] can mitigate this problem. This electrically thin dielectric layer located in the close vicinity above a phased array antenna by supporting a leaky wave that enhances the radiation toward a fixed direction compensates the scan loss. Different types of WAIM structure have been subsequently investigated, using artificial dielectrics or metamaterials to improve the performance, either in scanning range or operational bandwidth [4], [5], [6]. Similarly, an array of isotropic elements phased to first focus in the near-field will naturally radiate a wide far-field beam. However, to achieve a good beam efficiency over a limited angular range, the element pattern of each radiator can be controlled by the superstrate supported leaky wave.

In this work, we investigate the possibility of enhancing the radiation of single and multiple slot antennas by means of a WAIM realized using artificial dielectrics layers (ADLs). Being planar and very close to the array plane, the WAIM can be integrated with the array in a single printed circuit board (PCB). A dispersion analysis of the leaky modes supported by the ADLs is presented, as well as a tradeoff analysis between off-broadside gain enhancement and interelement mutual coupling. These studies are computationally very efficient by exploiting closed-form expressions to describe artificial dielectrics in the spectral domain [7], [8], [9], [10]. The artificial dielectric superstrate supports leaky waves that can be optimized to enhance the gain in a specific angular region [11], [12], [13], [14]. The same concept was originally proposed mainly within the scope of obtaining highly directive

Manuscript received 30 April 2022; revised 11 August 2022; accepted 11 October 2022. Date of publication 26 October 2022; date of current version 19 January 2023. This work was supported by the Dutch Technology Foundation NWO-TTW [WAtt LEvel transmitters at mm-waves (WhALE, 15591)], as part of the TTW-NXP Partnership Programme "Advanced 5G Solutions." *(Corresponding author: Ralph M. van Schelven.)*

Ralph M. van Schelven, Waqas H. Syed, Giorgio Carluccio, Kostas Doris, and Anton de Graauw are with NXP Semiconductors, 5656 AE Eindhoven, The Netherlands (e-mail: ralph.van.schelven@nxp.com).

Andrea Neto and Daniele Cavallo are with the Microelectronics Department, Electrical Engineering, Mathematics and Computer Science Faculty, Delft University of Technology, 2628 CD Delft, The Netherlands.

Color versions of one or more figures in this article are available at https://doi.org/10.1109/TAP.2022.3217340.

Digital Object Identifier 10.1109/TAP.2022.3217340

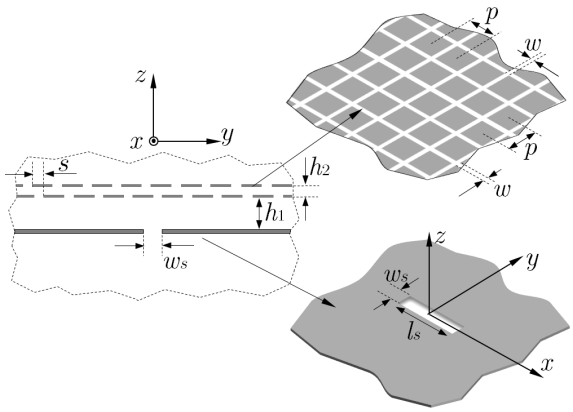

Fig. 1. Slot in the presence of an ADL superstrate, with the characteristic geometrical parameters.

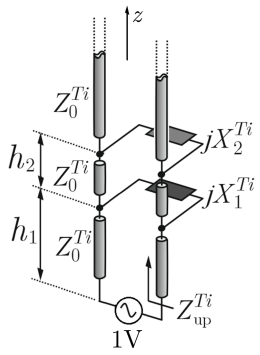

Fig. 2. Transmission line equivalent circuit of a source in the presence of two ADLs, for both the TE and TM waves.

radiation [15]. As typical for WAIM or leaky wave antennas, the bandwidth of operation is inversely proportional to the leaky wave angle of radiation from broadside. Accordingly, since here we target relatively wide field of view of $\pm 45°$, a design tradeoff between bandwidth and scan angle is shown in this article to reach approximately 13% relative bandwidth, defined as -1 dB gain variation.

II. Slot With ADL Superstrate in Free Space

To illustrate the antenna concept, we first assume that the slot radiators and the ADL superstrate are in free space. Although not physically realizable, this ideal case allows highlighting the main radiation mechanism.

A. Single Slot

The geometry under consideration is shown in Fig. 1 and consists of a slot oriented along x, in the presence of a two-layer ADL superstrate. Each ADL is realized as a doubly periodic array of electrically small square patches. The period p is assumed to be smaller than a quarter wavelength, within the frequency band of investigation. The width of the gaps between the patches is w, and the relative shift between the top and bottom layers is s. The distance between the slot plane and the bottom ADL is h_1 and the distance between the two ADLs is h_2. The slot is assumed to be electrically narrow, with width w_s, much smaller than the wavelength, while the slot length is indicated as l_s. For the calculation of the directivity and radiation patterns, only the upper hemisphere is considered in this section. For example, this can be realized in practice with a cavity-backed slot, which radiates only in the upper half-space.

When the ADLs are illuminated by a near source rather than a plane wave, the procedure presented in [7] can be used to evaluate the far-field of the source in the presence of the ADLs. The approach involves expanding the radiated field from the source in a spectrum of plane waves and using the equivalent transmission line model in Fig. 2. For each plane wave, characterized by the wavenumbers k_x and k_y along the x- and y-directions, the propagation constant on the line is given by $k_z = (k_0^2 - k_\rho^2)^{1/2}$, where k_0 is the free space wavenumber and $k_\rho^2 = k_x^2 + k_y^2$. Z_0^{Ti} is the characteristic impedance of the transmission lines for either the transverse magnetic (TM) or the transverse electric (TE) modes: $Z_0^{TM} = \zeta_0 k_z/k_0$ and $Z_0^{TE} = \zeta_0 k_0/k_z$, where $\zeta_0 = 120\pi\ \Omega$. The ADLs are represented in the circuit by two shunt reactances (X_1^{Ti} and X_2^{Ti}), where Ti can refer to either TM or TE components of the wave. This circuit allows to define the spectral dyadic Green's function of ADL stratification, which can be derived from the current and voltage solutions of these transmission lines when fed by a unit voltage generator at $z = 0$. If we assume the two layers to be identical, the equivalent reactance X^{Ti} is known in closed-form as a function of the geometrical parameters [8]

$$X^{TM} = \frac{-1}{B}, \quad X^{TE} = \frac{-1}{B\left(1 - \frac{k_\rho^2}{2k_0^2}\right)} \tag{1}$$

where B is the susceptance of the layers, given by

$$B = j\omega\varepsilon_0 \frac{p}{2\pi} \sum_{m\neq 0} \frac{|\mathrm{sinc}(\pi m \frac{w}{p})|^2}{|m|} F_m(h_2, p, s) \tag{2}$$

with

$$F_m(d_z, p, s) = -j - \cot\left(-j2\pi|m|\frac{h_2}{p}\right) + e^{j2\pi m\frac{s}{p}} \csc\left(-j2\pi|m|\frac{h_2}{p}\right). \tag{3}$$

The spectrum of the magnetic current on the slot is defined assuming a sinusoidal distribution in the longitudinal direction

$$M_l(k_x) = 2k_0 \frac{\cos(k_x l_s/2) - \cos(k_0 l_s/2)}{(k_0^2 - k_x^2)\sin(k_0 l_s/2)} \tag{4}$$

and edge-singular in the transverse direction

$$M_t(k_y) = J_0\big(k_y w_s/2\big) \tag{5}$$

where J_0 is the Bessel function of the first kind and zeroth order. The electric field in the far-field on a hemisphere with radius r_0 can be found for all the observation angles θ_0 and ϕ_0 using the stationary phase point approximation as

$$E_\xi(r_0, \theta_0, \phi_0) \approx jk_{z0} G_{\xi x}^{em}(k_{x0}, k_{y0}, z = h_1 + h_2) \times M_l(k_{x0}) M_t(k_{y0}) \frac{e^{-jk_0 r}}{2\pi r_0} \tag{6}$$

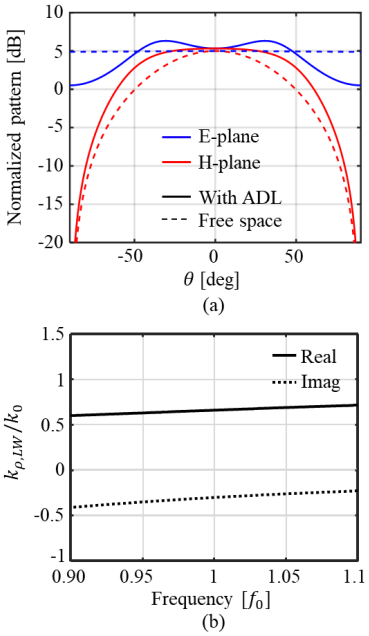

Fig. 3. (a) Normalized patterns of a slot in free space and in the presence of the ADL superstrate. The geometrical parameters of the structure are: $l_s = \lambda_0/2$, $w_s = \lambda_0/15$, $h_1 = 0.08\lambda_0$, $h_2 = 0.03\lambda_0$, $p = 0.2\lambda_0$, $w = 0.06\lambda_0$, and $s = 0.3\ p$. (b) Dispersion curve of the TM_0 leaky wave pole supported by the structure.

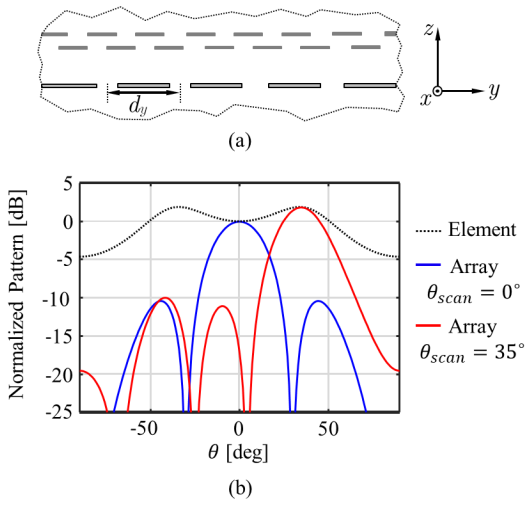

Fig. 4. (a) Array of four slots in the presence of an ADL superstrate in free space. The slots are displaced in the y-direction by a distance of $d_y = \lambda_0/2$. (b) Normalized radiation patterns of the array while scanning to broadside direction and to 35°. Also the element pattern shape is shown.

where ξ can refer to the x, y, or z component of the field, $k_{x0} = k_0 \sin\theta_0 \cos\phi_0$, $k_{y0} = k_0 \sin\theta_0 \sin\phi_0$, and $k_{z0} = k_0 \cos\theta_0$. $G_{\xi x}^{em}$ is the electric field Green's function in the ξ-direction due to x-oriented magnetic currents and is evaluated from the transmission line in Fig. 2, above the stratification ($z = h_1 + h_2$).

Fig. 3(a) shows the normalized patterns of the slot in the presence of the ADLs at a single frequency $f = f_0$ in the two principal planes. The geometrical parameters of the structure are: $l_s = \lambda_0/2$, $w_s = \lambda_0/15$, $h_1 = 0.08\lambda_0$, $h_2 = 0.03\lambda_0$, $p = 0.2\lambda_0$, $w = 0.06\lambda_0$, and $s = 0.3\ p$, where λ_0 is the free space wavelength at f_0. The normalized patterns of the slot in free space, i.e., without the ADL superstrate, is also shown as a reference.

A clear increase in normalized patterns in the E-plane is visible toward $\theta = \pm 35°$, which corresponds to the TM_0 leaky wave supported by the structure. Fig. 3(b) shows the dispersion curve of the leaky wave pole. The pole can be found by solving the dispersion equation $Z_{\text{up}}^{\text{TM}} = 0$, where $Z_{\text{up}}^{\text{TM}}$ is the impedance seen upward from the slot through the TM transmission line model of the stratification, as shown in Fig. 2. The sign of the square root $k_z = \pm(k_0^2 - k_\rho^2)^{1/2}$ is chosen such that we consider the poles of Green's function located on the bottom Riemann sheet. The angle of maximum radiation in the element pattern can be related to the leaky wave pole as [16]

$$\theta_{LW} = \tan^{-1}\left(\frac{Re\{k_{\rho,LW}\}}{Re\left\{\sqrt{k_0^2 - k_{\rho,LW}^2}\right\}}\right). \tag{7}$$

The imaginary part of the leaky wave pole is related to the attenuation constant of the leaky wave and can be used to determine the required distance between the slot and the truncated edges of the ADLs, such that diffraction from the edges of the structure becomes negligible.

Although a simple slot in free space has a constant radiation pattern in the E-plane and would therefore satisfy our requirement for a broad element pattern, this is not practically implementable. As the slot radiates the same amplitude toward ±90° as to broadside, the finiteness of the ground plane will cause significant diffraction and the pattern would be strongly dependent on the size of the ground plane. The ADL superstrate allows for an increase in gain toward a certain angle, while decreasing the power radiated to angles larger than θ_{LW}, making the patterns less sensitive to the truncation of the ground plane.

B. Array of Slots

We now consider the same slot element in an array configuration, as shown in Fig. 4(a). As an example, we consider four slots that are displaced by a distance d_y in the y-direction and fed with a linear phase shift for scanning in the E-plane. This number of elements is realistic considering the limited number of channels coming from a mm-wave chip. Fig. 4(b) shows the normalized radiation pattern of the array of four slots, with $d_y = \lambda_0/2$. The pattern is shown for broadside and scanning to 35°. Also the element pattern as designed in Section II-A is shown. By applying a phase shift between the individual antenna excitations, the resulting radiation pattern can be found by multiplying the array factor with the element pattern. It can be seen that the leaky waves characterizing the element patterns can be used to enhance the directivity of the array when scanning in specific directions.

To implement a variable beamwidth, instead of applying a linear phase shift between the excitation of the four slots, one can apply a quadratic phase distribution [17], placing a virtual focus point behind the array, as shown in Fig. 5(a). This configuration creates a diverging pattern that realizes a large

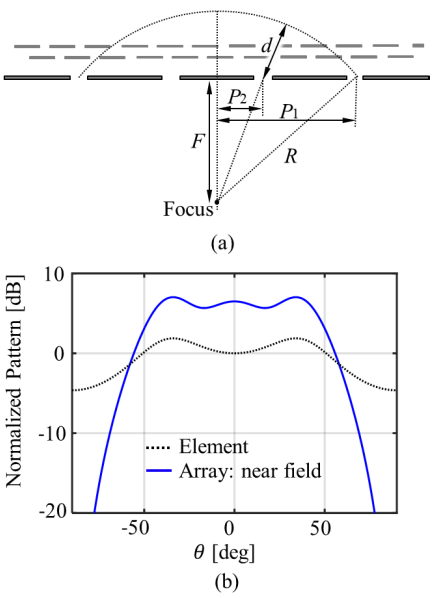

Fig. 5. (a) Geometry of the array for the quadratic phase shift. (b) Normalized radiation patterns of a single slot and of the array of four slots while focusing in the near-field.

beamwidth. For the four-element array, the phase difference between the outer and inner elements can be calculated by assuming virtual sources located along a circle centered around a focus point. This is achieved by applying a phase shift to the inner elements equal to $\beta_q = k_0\, d$, where $d = R-(P_2^2+F^2)^{1/2}$ is the distance between the inner elements and the circle and $R = (P_1^2+F^2)^{1/2}$ is the radius of the circle. This is combined with a tapered amplitude of the excitations $A = [0.6\ 1\ 1\ 0.6]$, to reduce the oscillations in the pattern. In the array under consideration, $P_1 = 1.5d_y$ and $P_2 = 0.5d_y$. Fig. 5(b) shows the pattern of the array with a phase distribution of $\phi = [0^\circ\ 101^\circ\ 101^\circ\ 0^\circ]$ (corresponding to $F = 0.7\lambda_0$), normalized to the broadside value of the isolated element pattern, which is also shown. It can be seen that by applying a quadratic phase shift between the elements, the pattern of the array is still wide and the amplitude is about 6 dB higher than that of an isolated element resulting in higher transmitted power.

By switching between the linear phase shift and the near-field focus, the same array can be used both to scan to large angle with enhanced gain and to have a wide field of view.

III. Study on Gain Enhancement and Mutual Coupling

In Section II, only radiation properties were considered. However, as shown in [18] there is an immediate relationship between the maximum achievable gain from multiple slots and the mutual coupling.

Dielectric superstrates can be used to reduce the mutual coupling, as done for example in [19] and [20]. The strategy in those works was to optimize the distance between the antenna array and the superstrate such that the direct space wave between two elements and the leaky wave reflected by the superstrate would have opposite phase and cancel out.

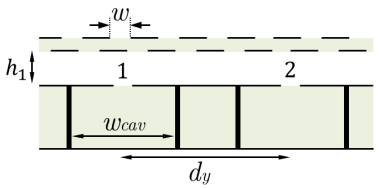

Fig. 6. Geometry under consideration for the study on the gain enhancement and the mutual coupling, consisting of cavity-backed slots with an ADL superstrate.

This cancellation requires relatively large distances between array and superstrate, in the order of half wavelength. On the contrary, in this work, we investigate much smaller height ($<\lambda/10$) between array and superstrate, which are required to increase the gain at wide angles away from broadside, for scan loss reduction. In such a configuration, the direct space wave and the leaky wave have similar phase at the neighboring slot and do not cancel out, and thus, the presence of the superstrate results in a direct increase in mutual coupling. This latter causes a deterioration of active impedance matching when scanning.

To address the tradeoff between gain enhancement at large angles and mutual coupling, a study is done, similar to the one presented in [18], for cavity-backed slots in the presence of the ADL superstrate, as shown in Fig. 6. The slots are oriented along x, and both the cavity-backed slots and the ADLs are considered to be printed on a dielectric with relative permittivity $\varepsilon_r = 3.5$. When including the dielectric layers, (1)–(4) can still be used, but replacing ε_0 and k_0 with ε_{av} and k_{av}, i.e., the average permittivity and wavenumber between the media above and below the ADL or the slot plane. A parametric study is performed, where the distance between the slot array and the ADL superstrate, h_1, is varied, as well as the effective refractive index of the ADL by varying the value of w. Since the slots are identical, the mutual coupling, S_{12}, is found from the mutual admittance as [21]

$$S_{12} = \frac{-2Y_{12}Y_0}{(Y_{11}+Y_0)^2 - Y_{12}^2} \tag{8}$$

where Y_0 is the normalization admittance of the two slots. The mutual admittance can be evaluated as a spectral integral as [18]

$$Y_{12} = \frac{-1}{(2\pi)^2}\int_0^{2\pi}\int_0^{\infty} |M(k_\rho,\alpha)|^2 G^{hm}_{xx,up}(k_\rho,\alpha) \times e^{-jk_\rho \cos(\alpha-\pi/2)d_y} k_\rho dk_\rho d\alpha \tag{9}$$

where $M(k_\rho,\alpha) = M_l(k_\rho,\alpha)M_t(k_\rho,\alpha)$ from (4) and (5), and k_ρ and α are related to the spectral variables k_x and k_y as $k_\rho = (k_x^2+k_y^2)^{1/2}$ and $\alpha = \tan^{-1}(k_y/k_x)$. $G^{hm}_{xx,up}$ is the x-component of the spectral Green's function for magnetic fields due to magnetic currents oriented along x, for the medium above the slots, which is found analytically as described in Section II (see Fig. 2), and d_y is the center-to-center distance between the slots.

The self-admittance can be computed as the sum of two terms

$$Y_{11} = Y_{11,up} + Y_{11,down} \tag{10}$$

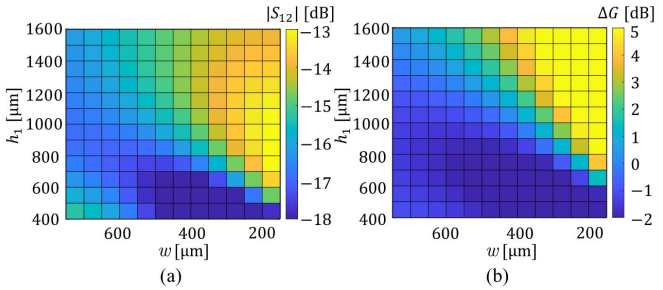

Fig. 7. (a) S_{12} and (b) ΔG of the element pattern of the cavity-backed slots in the presence of the ADL superstrate while varying h_1 and w.

with

$$Y_{11,up} = \frac{-1}{(2\pi)^2}\int_0^{2\pi}\int_0^{\infty} |M(k_\rho,\alpha)|^2 G^{hm}_{xx,up}(k_\rho,\alpha) k_\rho dk_\rho d\alpha \tag{11}$$

and

$$Y_{11,down} = \frac{-1}{2\pi}\int_{-\infty}^{\infty}\frac{1}{w_{cav}} \times \sum_{m=-\infty}^{\infty} |M_t(k_{ym})|^2 G^{hm}_{xx,down}(k_x,k_{ym})|M_l(k_x)|^2 dk_x \tag{12}$$

with $k_{ym} = -(2\pi m)/w_{cav}$ being the wavenumbers of the Floquet modes accounting for the periodic nature in the y-direction enforced by the cavity side walls [22]. $G^{hm}_{xx,down}$ is the x-component of the spectral Green's function of the stratification below the slots. For a fair comparison of S_{12}, one must make sure that the slots are well-matched, and therefore, we impose $Y_0 = Y_{11}$. Besides, the mutual coupling, the gain enhancement, defined as $\Delta G = G(45°) - G(0°)$, is found from the isolated element patterns for every h_1 and w.

Fig. 7 shows the resulting S_{12} and ΔG at a frequency of 30 GHz, while varying h_1 from 400 to 1600 μm, and w from 750 to 1504 μm. This variation in w corresponds to a variation in the effective refractive index of the ADL from 2.5 to 5. The other geometrical parameters are: $l_s = 5$ mm, $w_s = 0.2$ mm, $w_{cav} = 1.3$ mm, $d_y = 5$ mm, $h_2 = 0.2$ mm, $p = 1.2$ mm, and $s = 0$. Comparing the maps in Fig. 7(a) and (b), it can be seen that a gradient of increasing ΔG corresponds to increasing values of mutual coupling. During the design phase, it was observed that geometries resulting in a mutual coupling between two elements above -15 dB lead to large variations in the active input impedance of the four-element array when scanning in a $\pm 45°$ angular range. Therefore, from this simplified study of a two-element array, combinations of the parameters h_1 and w that provide a mutual coupling of -15 dB or lower are considered for the design. For these values of S_{12}, the gain difference is close to 0 d B for lower values of h_1 and increasing to about 2 dB for higher values of h_1. However, larger distances from ADL also yield to more dispersive patterns and larger impedance variation with the frequency.

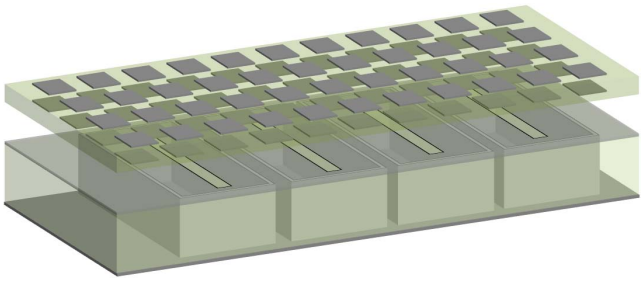

Fig. 8. Geometry of the array of cavity-backed slots in the presence of an ADL superstrate.

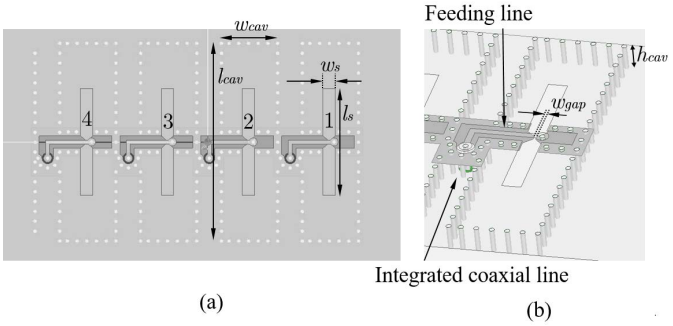

Fig. 9. (a) Top view of the slot array. (b) 3-D view of an array element with feeding structure.

IV. Array Design

An array design operating around 30 GHz is presented in this section, based on the schematic geometry shown in Fig. 8. It consists of four cavity-backed slot antennas in the presence of a two-layer ADL superstrate separated by an air gap. Both the array and the ADL superstrate can be fabricated using the standard PCB technology, where a foam layer can be used to realize the air gap between the slots and the ADL.

A more detailed figure of the designed array is shown in Fig. 9. Based on the tradeoff presented in Section III, the following geometrical parameters are derived: $l_s = 6.6$ mm, $w_s = 0.75$ mm, $w_{cav} = 3.4$ mm, $l_{cav} = 12.2$ mm, and $h_{cav} = 1$ mm. The cavity is realized with via walls and the slot is fed with a grounded co-planar waveguide (GCPW), which in turn is connected to an integrated coaxial line to reach the feeding network below the ground plane. The GCPW is terminated on a short circuit with a via, where the slot is tapered to a narrower width $w_{gap} = 100$ μm. The total size of the slot plane and the ADLs in the x- and y-directions is 7.5 mm $\times$ 17 mm.

The dimensions of the ADLs are $p = 1.2$ mm, $w = 0.4$ mm, and $s = 0$. The layer stack-up of the demonstrator board is shown in Fig. 10(a). Three versions of the demonstrator are realized with different feeding networks to achieve various radiation cases, i.e., broadside, scanning to 45° and the wide beam. The broadside, scanning, and broad beam feeding networks are shown in Fig. 10(b)–(d), respectively.

Fig. 11 shows the active S-parameters of the four individual slots for the three different excitations under consideration. It can be seen that a -10 dB impedance matching is achieved in the band from 29 to 31 GHz. The simulated radiation

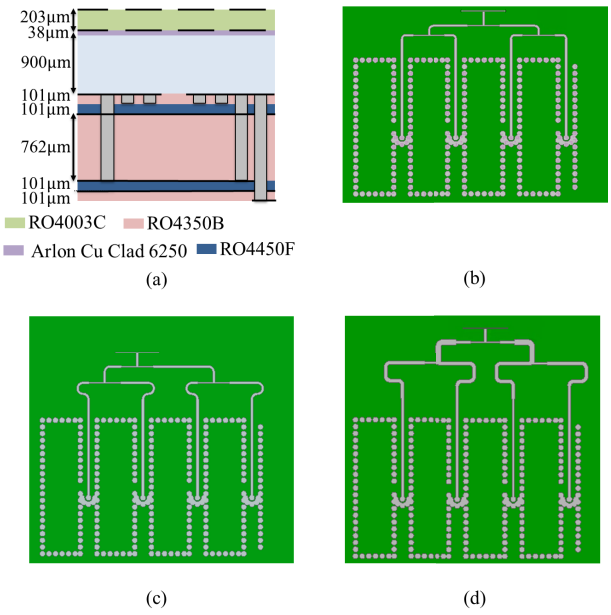

Fig. 10. (a) Stack-up of the demonstrator board. Bottom views of (b) broadside, (c) scanning, and (d) broad beam boards, showing the feeding networks.

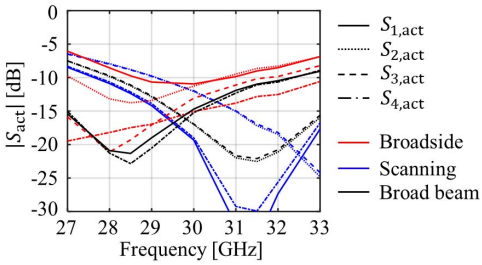

Fig. 11. Magnitude of the active S-parameters of the four individual antenna elements for the broadside beam, while scanning and for the broad beam.

patterns of the array for the three different excitations are shown in Fig. 12. For the broadside array, both the E- and H-plane patterns are shown for 30 GHz in Fig. 12(a), while the E-plane patterns for multiple frequencies are shown in Fig. 12(b). The E-plane patterns at different frequencies are reported in Fig. 12(c) and (d), for scanning to 45° and for the wide beam case, respectively. It can be observed that the patterns are stable with frequency within the band of investigation. Also, when comparing Fig. 12(b) and (c), it can be seen that the gain while scanning to 45° is approximately equal to the gain for broadside scanning, as targeted by the design. Fig. 12(d) shows that the same array can be used to generate a broad pattern when exciting all the four slots with a quadratic phase distribution, thus increasing the effective isotropic radiated power compared with exciting a single slot of the array. The feeding network is designed to achieve a voltage amplitude taper of $A = [0.6\ 1\ 1\ 0.6]$ and a phase distribution of $\phi = [0°\ 106°\ 106°\ 0°]$. The quadratic phase distribution and the amplitude taper can be optimized to obtain a flat top hat pattern at a certain frequency. However, due to the frequency dispersion of the patterns a slight dip in the broadside direction appears at other frequencies within the band.

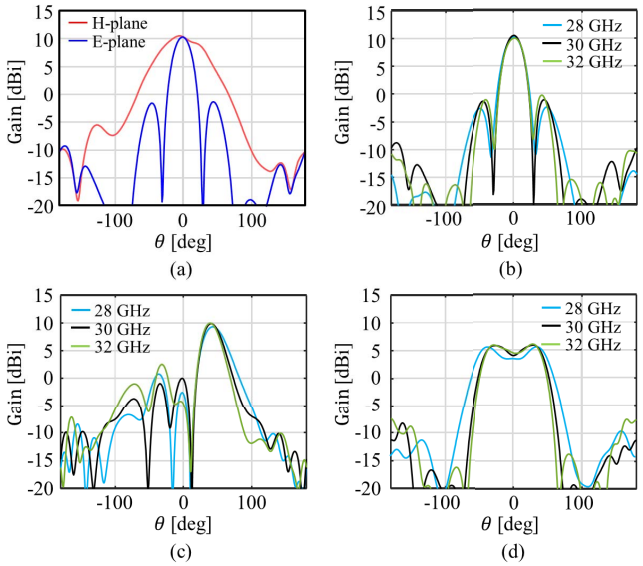

Fig. 12. Gain patterns of the four-element array for (a) broadside scanning (both E- and H-planes) at 30 GHz, and for multiple frequencies around the band of interest for (b) broadside scanning, (c) scanning toward 45° in the E-plane, and (d) near-field focus in the E-plane.

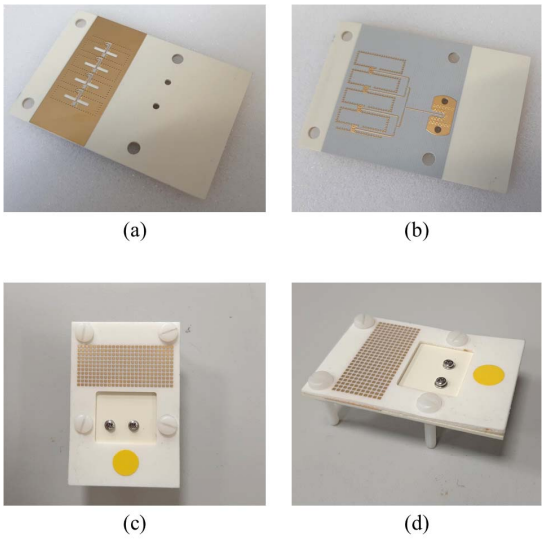

Fig. 13. Photographs of fabricated demonstrator boards. (a) Top view of array without ADL superstrate. (b) Bottom view of broadside board. (c) Top view of assembled PCBs. (d) Overview of assembled PCBs.

V. Measurements

Three prototype demonstrator boards have been manufactured for the experimental validation of the design. Each board has a different feeding network implemented to excite the array, as shown in Fig. 10, to realize a narrow beam to broadside and 45° as well as the broad beam. The three boards for the three different excitation modes are fabricated in the standard PCB technology. The photographs of the PCB are presented in Fig. 13. The artificial dielectric superstrate is fabricated as a separate board and can be attached on top of the three slot arrays.

Top mounted solderless Rosenberger 02K722-40MS3 50 Ω PCB connectors [23] are used to connect to the input of the feeding networks. The array and the broadside feeding network

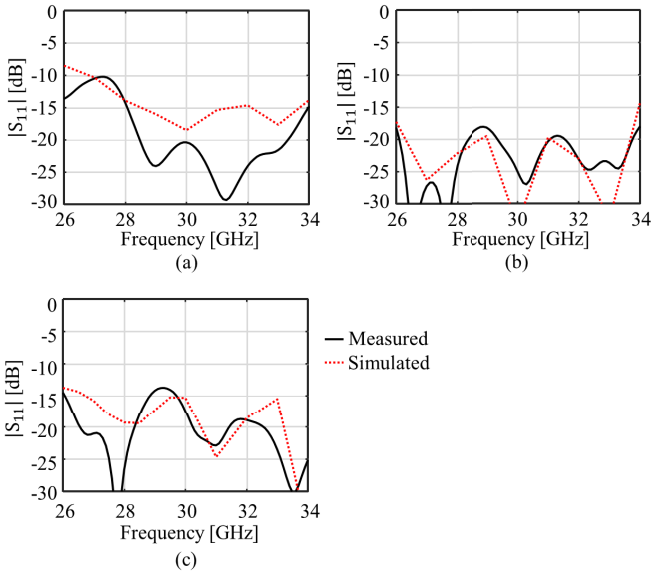

Fig. 14. Measured magnitude of the S-parameters of the three boards. (a) Broadside, (b) scanning, and (c) broad beam.

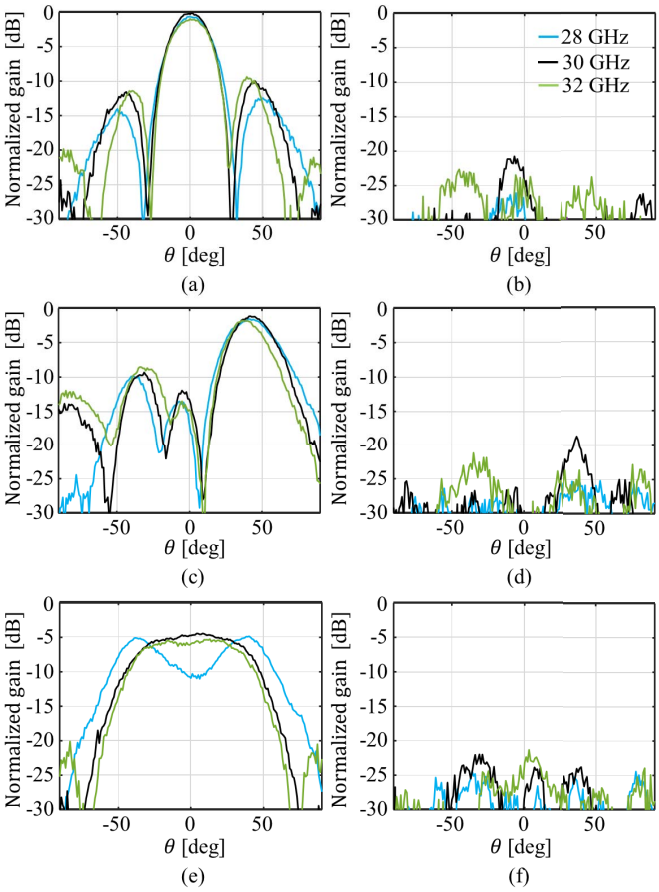

Fig. 15. Measured and normalized E-plane patterns of the array for several frequencies in broadside direction (a) co- and (b) cross pol., scanning to 45° (c) co- and (d) cross pol., and the wide beam (e) co- and (f) cross pol. All patterns are normalized to the maximum of broadside array at 30 GHz.

can be seen in Fig. 13(a) and (b), where as Fig. 13(c) and (d) show pictures of the assembled boards with the ADL superstrate. A back-to-back version of the feeding network has also been manufactured to assess the losses of the feeding lines.

The measured and simulated reflection coefficients of the three boards are shown in Fig. 14. The roughness of copper is included in the simulation performed in HFSS using the Groiss method [24], with a root mean square roughness of 2.8 μm [25]. The S-parameters from all the three boards show a fair agreement with simulations, given the typical tolerances of mm-wave PCBs. The observed differences, especially in 14(a), could also be explained with a small underestimation of losses in the simulation compared with the measurements. Moreover, an accurate characterization of the connector was not performed, which can result in additional measurement errors. It is worth to note that the reflection coefficients in Fig. 14 are lower than the previously presented levels at the slot terminals in Fig. 11, because of the added losses of the feeding networks.

Fig. 15 shows the measured normalized E-plane patterns (co- and cross-polarizations) for the three excitations for several frequencies. All the patterns are normalized to the maximum of broadside array at 30 GHz. It can be seen that the patterns while pointing to the broadside direction [see Fig. 15(a)] and while scanning to 45° [see Fig. 15(c)] are stable with frequency, whereas the broad beam [see Fig. 15(e)] shows more variations. This is in line with the simulated patterns as shown in Fig. 12. Also it can be seen that the measured amplitude for the broadside case and while scanning is approximately equal, and the broad beam is around 5 dB lower, again as is expected from simulation (see Fig. 12). Finally, it can be seen that the cross-polarization amplitude for all the three excitation cases is lower than -20 dB.

A comparison between the normalized patterns from the simulation and from the measurements at 30 GHz is shown in Fig. 16. A good agreement can be seen for the broadside case, both for the E- and H-planes, and while scanning to 45°. For the broad beam, some discrepancy can be observed between the measured and simulated patterns, since the measured beam appears to be slightly narrower and does not exhibit the two-peak characteristics of the simulated pattern.

To explain this difference in the patterns, a tolerance study is performed on several parameters, according to the information provided by the manufacturer and from the material datasheets: h_1 is varied from the nominal value in the range ± 200 μm, w is ± 50 μm, the amplitude of the elements is ± 2 dB, and the phase of the elements is $\pm 15°$. Also the dielectric constant of the Rohacell foam is varied from $\varepsilon_r = 1$ to 1.2. Fig. 17 shows several patterns in gray obtained by varying the parameters, compared with the measured pattern in black. It can be seen that the tolerances can explain the discrepancy as the black curve falls within the range of gray patterns.

Fig. 18(a) reports a comparison between the simulated and measured values of the gain as a function of frequency for the broadside array, showing a good agreement. The losses of the broadside feeding network are shown in Fig. 18(b), both from the simulations and measurements. The feeding network losses are measured by means of a back-to-back structure as in the inset of Fig. 18(b) and divided by 2 to account only for half

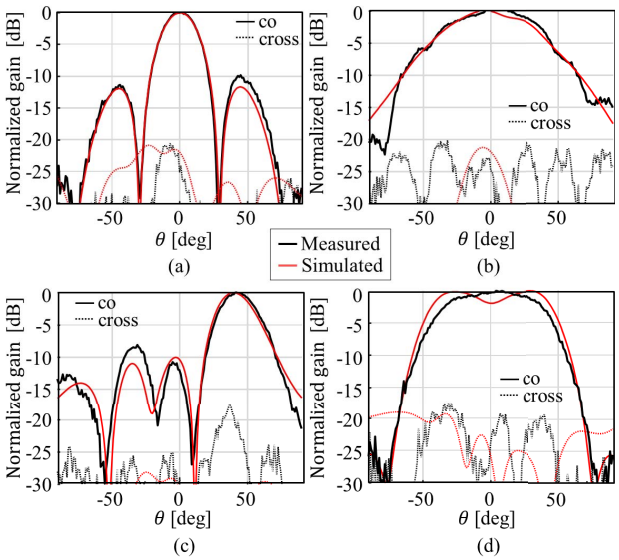

Fig. 16. Comparison between normalized patterns from HFSS and measurements for the broadside case (a) E- and (b) H-plane, (c) E-plane while scanning to 45°, and (d) E-plane for the broad beam.

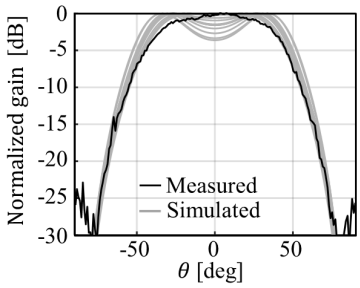

Fig. 17. Tolerance study on the pattern of the broad beam. The considered parameters are: h_1, w, A, ε_r of the foam, and the phase distribution along the array.

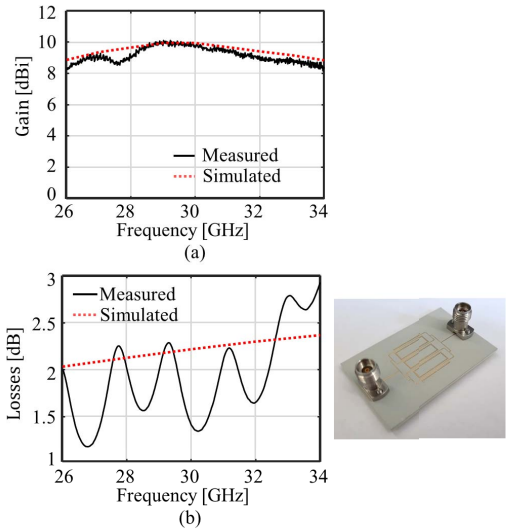

Fig. 18. (a) Comparison between the simulated and measured values of the gain and the realized gain for the broadside array. (b) Measured ohmic losses of the broadside feeding network.

of the transition. The oscillatory behavior in the measurement is due to some reflection occurring at the connectors, which is not accounted for in the simulations. It can be seen that approximately 1.3–2.3 dB of losses can be attributed to the feeding network in the band 28–32 GHz.

VI. Conclusion

We presented a study of planar slot antennas with artificial dielectric superstrates to realize pattern shaping. Based on the analysis of leaky waves propagating along the artificial dielectric slab, the shape of the element pattern can be manipulated to enlarge the beamwidth. When used in array configuration, such an element can achieve reduced scan loss. The same array can also be used to radiate a pattern with large beamwidth using quadratic phase illumination.

A study was done on the relationship between the gain difference between broadside and 45° due to the leaky waves and the mutual coupling between antenna elements within an array. This study led to a tradeoff between matching and scan performance. An array design with a stable gain (gain difference ≈0 dB) in the scan range ±45° was concluded to be a good tradeoff between impedance matching and radiation performance.

A PCB prototype of the array for 30 GHz operation was manufactured and tested. Three arrays were fabricated, with different feeding networks to realize a beam in broadside direction, scanning to 45° and a broad beam. The measured results showed a good agreement with simulations, with a gain variation as a function of scan angle and frequency of less than 1 dB within a ±45° field of view and a 28–32 GHz bandwidth.

The proposed array concept has potential to be used in multimode mm-wave phased array with electronic control of phase and amplitudes of the elements.

Acknowledgment

The authors would like to thank Pascal Aubry for kindly aiding in the measurements of the prototypes in the anechoic chamber.

References

[1] E. Kruglick, "Network coverage by cycling through beam shape coverage configurations," Patent WO 0 28 187 Al, Feb. 8, 2013.

[2] D. R. Jackson and A. A. Oliner, "A leaky-wave analysis of the high-gain printed antenna configuration," *IEEE Trans. Antennas Propag.*, vol. AP-36, no. 7, pp. 905–910, Jul. 1988.

[3] E. Magill and H. Wheeler, "Wide-angle impedance matching of a planar array antenna by a dielectric sheet," *IEEE Trans. Antennas Propag.*, vol. AP-14, no. 1, pp. 49–53, Jan. 1966.

[4] C.-C. Chen, "Wideband wide-angle impedance matching and polarization characteristics of circular waveguide phased arrays," *IEEE Trans. Antennas Propag.*, vol. AP-22, no. 3, pp. 414–418, May 1974.

[5] T. R. Cameron and G. V. Eleftheriades, "Analysis and characterization of a wide-angle impedance matching metasurface for dipole phased arrays," *IEEE Trans. Antennas Propag.*, vol. 63, no. 9, pp. 3928–3938, Sep. 2015.

[6] D. Cavallo, W. H. Syed, and A. Neto, "Connected-slot array with artificial dielectrics: A 6 to 15 GHz dual-pol wide-scan prototype," *IEEE Trans. Antennas Propag.*, vol. 66, no. 6, pp. 3201–3206, Jun. 2018.

[7] D. Cavallo, W. H. Syed, and A. Neto, "Closed-form analysis of artificial dielectric layers—Part II: Extension to multiple layers and arbitrary illumination," *IEEE Trans. Antennas Propag.*, vol. 62, no. 12, pp. 6265–6273, Dec. 2014.

[8] D. Cavallo and C. Felita, "Analytical formulas for artificial dielectrics with nonaligned layers," *IEEE Trans. Antennas Propag.*, vol. 65, no. 10, pp. 5303–5311, Oct. 2017.

[9] D. Cavallo, "Dissipation losses in artificial dielectric layers," *IEEE Trans. Antennas Propag.*, vol. 66, no. 12, pp. 7460–7465, Dec. 2018.
[10] D. Cavallo and R. M. van Schelven, "Closed-form analysis of artificial dielectric layers with non-periodic characteristics," in *Proc. 13th Eur. Conf. Antennas Propag. (EuCAP)*, 2019, pp. 1–5.
[11] R. Gardelli, M. Albani, and F. Capolino, "Array thinning by using antennas in a Fabry–Perot cavity for gain enhancement," *IEEE Trans. Antennas Propag.*, vol. 54, no. 7, pp. 1979–1990, Jul. 2006.
[12] A. Neto, N. Llombart, G. Gerini, M. D. Bonnedal, and P. de Maagt, "EBG enhanced feeds for the improvement of the aperture efficiency of reflector antennas," *IEEE Trans. Antennas Propag.*, vol. 55, no. 8, pp. 2185–2193, Aug. 2007.
[13] A. Neto, M. Ettorre, G. Gerini, and P. De Maagt, "Leaky wave enhanced feeds for multibeam reflectors to be used for telecom satellite based links," *IEEE Trans. Antennas Propag.*, vol. 60, no. 1, pp. 110–120, Jan. 2012.
[14] D. Blanco, N. Llombart, and E. Rajo-Iglesias, "On the use of leaky wave phased arrays for the reduction of the grating lobe level," *IEEE Trans. Antennas Propag.*, vol. 62, no. 4, pp. 1789–1795, Apr. 2014.
[15] G. V. Trentini, "Partially reflecting sheet arrays," *IRE Trans. Antennas Propag.*, vol. 4, no. 4, pp. 666–671, Oct. 1956.
[16] F. Monticone and A. Alù, "Leaky-wave theory, techniques, and applications: From microwaves to visible frequencies," *Proc. IEEE*, vol. 103, no. 5, pp. 793–821, May 2015.
[17] R. C. Hansen, "Focal region characteristics of focused array antennas," *IEEE Trans. Antennas Propag.*, vol. AP-33, no. 12, pp. 1328–1337, Dec. 1985.
[18] N. Llombart, A. Neto, G. Gerini, M. Bonnedal, and P. D. Maagt, "Impact of mutual coupling in leaky wave enhanced imaging arrays," *IEEE Trans. Antennas Propag.*, vol. 56, no. 4, pp. 1201–1206, Apr. 2008.
[19] K.-L. Wu, C. Wei, X. Mei, and Z.-Y. Zhang, "Array-antenna decoupling surface," *IEEE Trans. Antennas Propag.*, vol. 65, no. 12, pp. 6728–6738, Dec. 2017.
[20] Y. Da, Z. Zhang, X. Chen, and A. A. Kishk, "Mutual coupling reduction with dielectric superstrate for base station arrays," *IEEE Antennas Wireless Propag. Lett.*, vol. 20, no. 5, pp. 843–847, May 2021.
[21] D. M. Pozar, *Microwave Engineering*, 4th ed. Hoboken, NJ, USA: Wiley, 2012.
[22] W. H. Syed, D. Cavallo, H. T. Shivamurthy, and A. Neto, "Wideband, wide-scan planar array of connected slots loaded with artificial dielectric superstrates," *IEEE Trans. Antennas Propag.*, vol. 64, no. 2, pp. 543–553, Feb. 2016.
[23] Rosenberger. *02K722-40MS3*. Technical Data Sheet. Accessed: Jul. 22, 2021. [Online]. Available: https://products.rosenberger.com/_ocassets/db/02K722-40MS3.pdf
[24] S. Groiss, I. Bardi, O. Biro, K. Preis, and K. R. Richter, "Parameters of lossy cavity resonators calculated by the finite element method," *IEEE Trans. Magn.*, vol. 32, no. 3, pp. 894–897, May 1996.
[25] Rogers Corporation. *Copper Foils for High Frequency Materials*. Accessed: Jul. 22, 2021. [Online]. Available: http://payalnik.com.ua/upload/docum/Copper-Foils-for-High-Frequency-Circuit-Materials.pdf

Ralph M. van Schelven received the B.Sc. and M.Sc. degrees *(cum laude)* in electrical engineering and the Ph.D. degree in electromagnetics from the Delft University of Technology (TU Delft), Delft, The Netherlands, in 2015, 2017, and 2022, respectively.

He is currently an Antenna Engineer with NXP Semiconductors, Eindhoven, The Netherlands. His research interests include antenna-in-package and the design of integrated mm-wave solutions.

Dr. van Schelven was a recipient of an Honorable Mention at the IEEE Antennas and Propagation Society International Symposium in 2019.

Waqas H. Syed received the B.Sc. degree (Hons.) in telecommunication engineering from the COMSATS Institute of Information Technology, Islamabad, Pakistan, in 2007, the M.Sc. degree from RWTH Aachen University, Aachen, Germany, in 2010, and the Ph.D. degree *(cum laude)* in electromagnetics from the Delft University of Technology (TU Delft), Delft, The Netherlands, in 2015.

From 2015 to 2016, he was a Post-Doctoral Researcher with the Terahertz Sensing Group, TU Delft. He is currently an Antenna Engineer with NXP Semiconductors, Eindhoven, The Netherlands. His current research interests include antenna-in-package, artificial dielectrics, and design of integrated antennas and arrays.

Dr. Syed was a recipient of the Special Mention for Excellent Presentation at the European Conference on Antennas and Propagation in 2015 and the 2016 Else Kooi Award for the Best Young Researcher in the field of applied semiconductor research and microelectronics conducted in The Netherlands.

Giorgio Carluccio (Member, IEEE) was born in 1979 and grew up in Ortelle, Italy. He received the Laurea degree in telecommunications engineering and the Ph.D. degree in information engineering from the University of Siena, Siena, Italy, in 2006 and 2010, respectively.

In 2008 and 2009, he was an Invited Visiting Scholar with the ElectroScience Laboratory, Department of Electrical and Computer Engineering, The Ohio State University, Columbus, OH, USA. From 2010 to 2012 and from 2013 to 2014, he was a Researcher with the Department of Information Engineering and Mathematics, University of Siena. From 2012 to 2013, he was a Researcher with the Department of Electronics and Telecommunication, University of Florence, Florence, Italy. In 2012 and 2013, he was a Visiting Researcher with the Department of Microelectronics, Delft University of Technology (TU Delft), Delft, The Netherlands, where he also was a Researcher from 2014 to 2018. Since 2018, he has been an RF Circuits and Antenna Scientist with NXP Semiconductors, Eindhoven, The Netherlands, where he focuses on RF devices for automotive radar applications. His research interests include electromagnetic wave theory, mainly focused on asymptotic high-frequency techniques for electromagnetic scattering and propagation; and with modeling and design of antennas, quasi-optical systems, and periodic structures: mainly reflector antennas, dielectric lens antennas, reflectarrays, connected arrays, THz antennas based on photoconductive materials, and antenna-in-package.

Dr. Carluccio was a recipient of the 2018 EurAAP International "Leopold B. Felsen Award for Excellence in Electrodynamics" and the 2010 URSI Commission B Young Scientist Award at the International Symposium on Electromagnetic Theory (EMTS 2010), where he also received the Third Prize for the Young Scientist Best Paper Award.

Kostas Doris (Member, IEEE) received the Ph.D. degree from the Technical University of Eindhoven, Eindhoven, The Netherlands, in 2004.

He is currently a fellow with NXP Semiconductors, Eindhoven, and a Professor with the Technical University of Eindhoven. He was with Philips Research Laboratories, Amsterdam, The Netherlands, and NXP Research, developing high-performance data converters for wireless and cable modem applications. Since 2012, he has been involved in mm-wave CMOS transceivers for automotive radars. He has (co-)authored multiple articles, patents, and books on data converters and RFCMOS radar.

Dr. Doris was an Associate Editor of the IEEE TRANSACTIONS OF CIRCUITS AND SYSTEMS, and the Technical Program Committee Member and the EU (Vice) Chair for the IEEE International Solid State Circuits Conference. Currently, he is serving as a Forum Champion.

Anton de Graauw was born in Delft, The Netherlands, in 1966. He received the M.Sc. degree in electrical engineering from the Technical University of Delft, Delft, in 1993.

He worked in several research and development positions at N.K.F. Telecom, Philips Components, Philips Semiconductors, and NXP Semiconductors, Eindhoven, The Netherlands, in the areas of fiber-optic CATV systems, RF and mm-Wave communication, and radar transceiver chips and antenna modules. He is currently an IC Architect in car-radar transceivers and integrated antennas at NXP Semiconductors.

Andrea Neto (Fellow, IEEE) received the Laurea degree *(summa cum laude)* in electronic engineering from the University of Florence, Florence, Italy, in 1994, and the Ph.D. degree in electromagnetics from the University of Siena, Siena, Italy, in 2000.

He was with the Antenna Section, European Space Agency Research and Technology Centre, Noordwijk, The Netherlands, for over two years. From 2000 to 2001, he was a Post-Doctoral Researcher with the California Institute of Technology, Pasadena, CA, USA, where he was with the Submillimeter Wave Advanced Technology Group. From 2002 to 2010, he was a Senior Antenna Scientist with the Netherlands Organization for Applied Scientific Research Defense, Security, and Safety, The Hague, The Netherlands. In 2010, he became a Full Professor of applied electromagnetism with the Department of Microelectronics, Delft University of Technology, Delft, The Netherlands, where he formed and currently leads the THz Sensing Group. His research interests include analysis and design of antennas with an emphasis on arrays, dielectric lens antennas, wideband antennas, EBG structures, and THz antennas.

Dr. Neto is a member of the Technical Board of the European School of Antennas and an Organizer of the course on THz antenna imaging. He was a recipient of the European Research Council Starting Grant to perform research on advanced antenna architectures for THz sensing systems in 2011 and the H. A. Wheeler Award for the Best Applications Paper in the IEEE TRANSACTIONS ON ANTENNAS AND PROPAGATION in 2008. He was the TPC Co-Chair for the Eucap 2021 Edition and the TPC Chair for the IRMMW-THz Conference in 2022. He served as an Associate Editor for the IEEE TRANSACTIONS ON ANTENNAS AND PROPAGATION from 2008 to 2013 and the IEEE ANTENNAS AND WIRELESS PROPAGATION LETTERS from 2005 to 2013 and an Associate editor of the *Transactions on THz Science and Technology*.

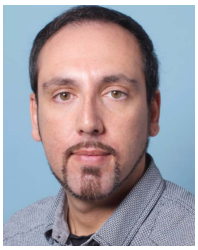

Daniele Cavallo (Senior Member, IEEE) received the M.Sc. degree *(summa cum laude)* in telecommunication engineering from the University of Sannio, Benevento, Italy, in 2007, and the Ph.D. degree *(cum laude)* in electromagnetics from the Eindhoven University of Technology, Eindhoven, The Netherlands, in 2011.

From 2007 to 2011, he was with the Antenna Group, Netherlands Organization for Applied Scientific Research, The Hague, The Netherlands. From 2012 to 2015, he was a Post-Doctoral Researcher with the Microelectronics Department, Delft University of Technology (TU Delft), Delft, The Netherlands, where he is currently an Associate Professor with the Terahertz Sensing Group. In 2015, he joined the Chalmers University of Technology, Gothenburg, Sweden, as a Visiting Researcher. He has authored or coauthored more than 150 papers published in peer-reviewed international journals and conference proceedings. His current research interests include analytical and numerical methods for antenna characterization, design of antenna arrays, and on-chip antennas.

Dr. Cavallo is a member of the European Association on Antennas and Propagation (EurAAP), a Co-Coordinator of the EurAAP Working Group "Active Array Antennas," and a Management Committee Member of the COST Action "Future communications with higher-symmetric engineered artificial materials (SyMat)." He was a recipient of the Best Innovative Paper Prize at the European Space Agency Antenna Workshop in 2008, the Best Paper Award in Electromagnetics and Antenna Theory at the 11th European Conference on Antennas and Propagation (EuCAP) in 2017, and the 250 keuro "Veni" Personal Grant from the Netherlands Organization for Scientific Research (NW0) in 2015. His students received the Best Student Paper Award at EuCAP 2013, the Special Mention at EuCAP 2015, the Else Kooi Prize in 2016, and the Honorable Mention at the IEEE Antennas and Propagation Society International Symposium in 2019. He is currently an Associate Editor of the IEEE TRANSACTIONS ON ANTENNAS AND PROPAGATION.